Femtosecond Chemistry

Edited by Jörn Manz and Ludger Wöste

Distribution:
VCH, P.O. Box 101161, D-69451 Weinheim (Federal Republic of Germany)
Switzerland: VCH, P.O. Box, CH-4020 Basel (Switzerland)
United Kingdom and Ireland: VCH (UK) Ltd., 8 Wellington Court, Cambridge CB1 1HZ (England)
USA and Canada: VCH, 220 East 23rd Street, New York, NY 10010-4606 (USA)
Japan: VCH, Eikow Building, 10-9 Hongo 1-chome, Bunkyo-ku, Tokyo 113 (Japan)

ISBN 3-527-29062-1

Weinheim · New York
Basel · Cambridge · Tokyo

12 Femtosecond Time-Resolved Photochemistry of Molecules and Metal Clusters

T. Baumert, R. Thalweiser, V. Weiss, G. Gerber

12.1 Introduction

Multiphoton ionization of small molecules has been studied in recent years by a variety of techniques and is generally well understood. The ionization is predominantly due to resonance-enhanced multiphoton ionization (REMPI) processes, whereas nonresonant multiphoton processes only start to play a role for higher laser intensities, in the range of gigawatts per square centimeter. Dynamical aspects of the interaction of laser radiation with molecules and details of the excitation and ionization processes can now be studied directly by femtosecond pump–probe techniques. This allows a closer look at the timescales of the absorption of several photons in molecular multiphoton ionization and the photofragmentation of neutral and ionic molecules.

Time-resolved measurements often open up new directions and provide a more general view of the primary physical and chemical processes. Due to recent developments in the generation of ultrashort light pulses, in particular the availability of the Ti : sapphire solid-state laser system with pulse durations as short as 10 fs, a broad range of new, exciting and formerly inconceivable real-time measurements are now possible. The observation of transient spectra together with an analysis using the wave-packet method gives very detailed information. Therefore, by studying ultrafast molecular and cluster dynamics with the femtosecond pump–probe techniques, we expect that many interesting and open issues can be solved or at least be better understood. However, sometimes studies even with a single femtosecond light pulse give surprising new results. We reported recently on the interaction of a bound, doubly excited, molecular state with different continua and the competition between the various decay channels [1]. In that study we used a femtosecond laser pulse as an experimental tool to distinguish between different multiphoton ionization pathways such as the dissociative ionization of the molecule and the neutral fragmentation with subsequent excited-fragment photoionization. Both processes are difficult to distinguish when using nanosecond or even picosecond laser pulses. This distinction is also of great importance in multiphoton ionization studies of metal-cluster systems.

The time-resolved multiphoton ionization and fragmentation of alkali-metal molecules, and in particular of Na_2 and Na_3, is of great interest. In many ex-

periments with Na_2 it has been found that, in conjunction with the formation of Na_2^+ ions, ionic fragments Na^+ are also formed. Resonance-enhanced multiphoton ionization (REMPI) processes via the $A\,^1\Sigma_u^+$ or the $B\,^1\Pi_u$ states are responsible for this observation. The sodium trimer Na_3, with its three vibrational modes, is a prototype system for the observation of a three-dimensional wave-packet motion. This trimer is probably spectroscopically the most studied and best known small metal-cluster [2]. Its excitation spectrum consists of several bands due to different excited electronic states, among which the B state with an onset at 625 nm is of greatest interest. This is because of the observed pseudorotational features in the spectra.

Zewail and coworkers [3] first demonstrated the enormous advantage of applying femtosecond lasers to the study of molecular dynamics. Their pioneering work in the field of femtosecond photochemistry and transient molecular fluorescence spectroscopy has initiated a number of other time-resolved ultrafast laser studies; see also Chapter 2.

In recent years, clusters and in particular metal clusters have been the fascinating subject of many experimental and theoretical studies. Clusters bridge the gap between surface physics and molecular physics. Metal clusters, in particular, show interesting features ranging from molecular properties seen in small particles to solid-state-like behavior of larger aggregates. Studies of cluster properties and the real-time dynamics of ionization and fragmentation have not yet been studied in detail as a function of cluster size. For related topics, see also Chapters 14 and 15.

In this chapter we present and discuss experimental results of time-resolved studies of molecular Na_2, Na_3, and metal-cluster Na_n ($n \leq 21$) ionization and fragmentation studies in beam experiments employing ion and electron spectroscopies together with femtosecond pump–probe techniques; see also Chapter 11 which covers theoretical considerations.

12.2 Experimental Studies

In our femtosecond laser molecular/cluster beam studies of time-resolved multiphoton ionization and fragmentation processes, we employ a combination of different experimental techniques. A supersonic molecular beam provides the molecules and clusters in a collision-free environment and restricts the initial states to the very lowest vibrational and rotational states. Our femtosecond lasers are used in a typical pump–probe arrangement. The pump laser initiates the dynamics under consideration, whereas the time-delayed probe laser monitors the temporal evolution of the system. As the probe laser usually ionizes the species, we can take full advantage of the powerful time-of-flight (TOF) technique in the detection part of our experiment. We use the mass resolution of the TOF spectrometer to study size-dependent cluster properties and to follow the product formation in a photodissociation process on the mass of individual products directly. If we wish to determine the final continuum states we can measure the time-resolved kinetic energy release in a photofragmentation process on the fragments of interest. In addition, the kinetic energy distribution

of ejected electrons and the ZEKE (zero-kinetic-energy) photoelectrons technique helps to clarify a specific ionization process (see also Chapter 4). In this combination of techniques, the supersonic molecular beam prepares the initial states and with the TOF technique the final states of the systems under consideration are determined. The femtosecond pump–probe lasers monitor the dynamics between the initial and final states. A sectional drawing of the molecular/cluster beam apparatus and the TOF spectrometers is shown in Fig. 12.1.

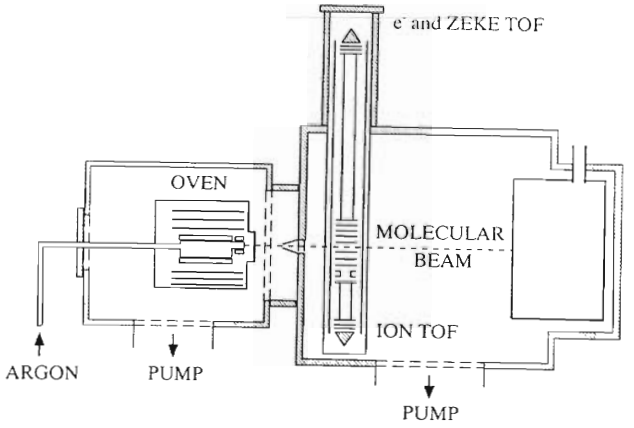

Figure 12.1 Sectional drawing of the molecular/cluster beam apparatus and the TOF spectrometers. The femtosecond lasers (not shown), the molecular/cluster beam axis and the spectrometer axis are all mutually perpendicular.

The supersonic sodium cluster/molecular beam is produced either by a pure sodium expansion through a small orifice of typically 0.10–0.15 mm diameter or by an expansion seeded with argon [4, 5]. The oven is usually operated at 1000 K with nozzle temperatures about 50 K higher. As an example, for a cylindrical nozzle of 0.2–0.3 mm length and 100 μm diameter we obtain vibrational temperatures of 80 K and rotational temperatures of 15 K for the sodium dimer at a seeding pressure of 6 bar.

Femtosecond light pulses are generated in two different home-built laser systems. Independently tunable femtosecond pulses of down to 50 fs duration and up to 50 μJ energy are generated in the laser system shown in Fig. 12.2. The tunability of our present system covers the near-UV, the complete visible range and the near-IR. The output pulses of a colliding-pulse mode-locked (CPM) ring dye laser [6, 7] are amplified in a bow-tie amplifier, which is pumped by an excimer laser at 308 nm, pulse-compressed and focused into a cell containing methanol to generate a white-light continuum. Alternative amplification schemes for ultrashort dye laser pulses are reviewed in [8], [9] and [10]. Pump and probe pulses at specific wavelengths are selected from the white-light continuum with a grating, which can also be used to

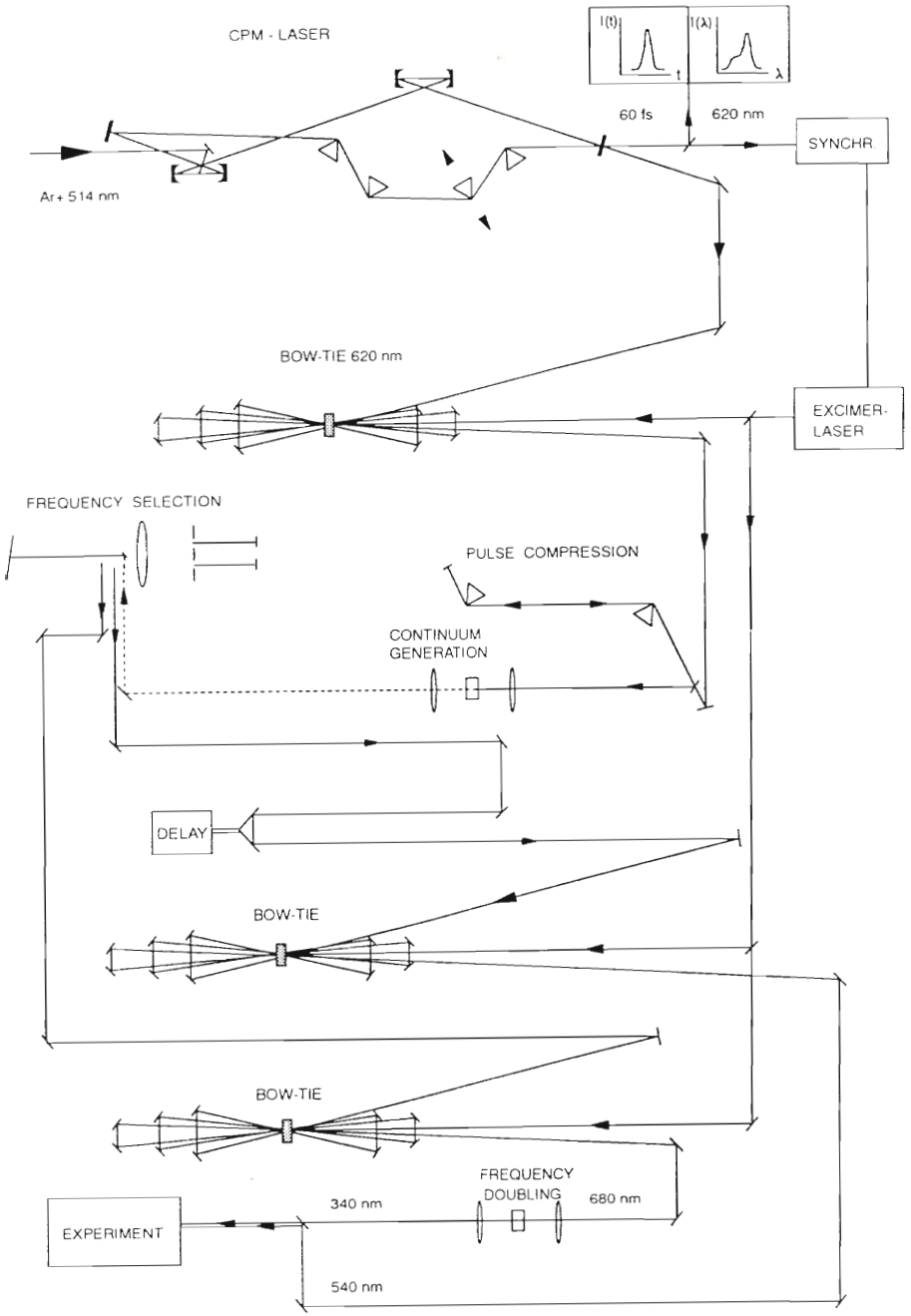

Figure 12.2 Femtosecond laser system for independently tunable pump and probe wavelengths.

compensate for group velocity dispersion in the subsequent amplification stages. Using adjustable slits for wavelength selection, the bandwidth of the pulses can be chosen depending upon the requirements of the experiment. Pump and probe pulses are amplified again in two additional bow-tie amplifiers. Additional wavelength conversion methods such as frequency doubling are used to generate tunable ultrashort UV-laser pulses. The pump and probe laser beams are recombined collinearly and focused into the interaction region. A Michelson arrangement is used to delay the probe laser relative to the pump laser. The ultimate phase-sensitive time resolution obtained with such a set-up is about 1 fs, as illustrated by the interferometric autocorrelation trace shown in Fig. 12.3.

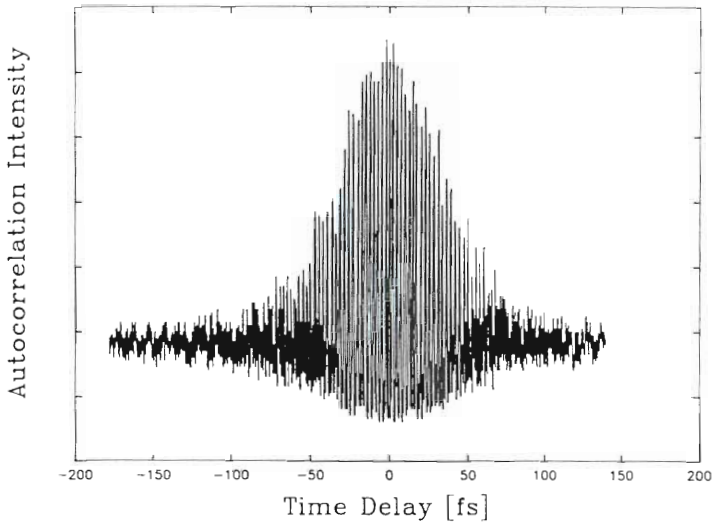

Figure 12.3 Interferometric autocorrelation of a Ti:Sapphire pulse at 773 nm, having a pulse duration of 40 fs sech^2. The autocorrelation trace displays the ultimate phase-sensitive time resolution of our set-up (in the order of 1 fs).

The second femtosecond laser system makes use of a home-built Ti:Sapphire laser oscillator. This Ti:sapphire laser produces light pulses of 20–70 fs time duration in the wavelength range 700–850 nm. Again using a bow-tie amplifier, pulse energies of the order of several 10 μJ are obtained. For a description of a recent Ti:Sapphire laser design which generates light pulses of 11 fs duration, see [11].

In our linear ion TOF spectrometer we achieve a mass resolution $m/\Delta m$ of about 70, which is sufficient to resolve the cluster masses under investigation. The kinetic energy release in dissociation processes is estimated as described, for example, in [12]. The energy resolution of our electron TOF spectrometer is 20 meV for electrons of 0.3 eV kinetic energy and 40 meV for electrons of 1.0 eV. With our ZEKE spec-

trometer, built according to the design of Müller-Dethlefs and Schlag [13], we achieve an energy resolution of 0.1 meV (or about 1 cm^{-1}).

12.3 Results and Discussion

12.3.1 Wave-Packet Motion in Molecular Multiphoton Ionization

12.3.1.1 Motivation

Typical molecular vibrational periods are of the order of several hundred femtoseconds. In order to investigate multiphoton ionization (MPI) mechanisms it is convenient, for several reasons, to apply laser pulses which are short in comparison with a vibrational period:

(a) In single-pulse experiments one can consider a molecular system to be frozen during the laser–molecule interaction time. Fragmentation with subsequent photoionization of the neutral fragment – leading to a blurred mass spectrum – is considerably suppressed in comparison with nanosecond and even picosecond laser experiments. This is especially important in cluster physics, as will be discussed later.

(b) Nanosecond laser REMPI experiments on rapidly dissociating systems often do not show the mass of the parent in the mass spectrum. Such systems, after absorbing a photon onto a dissociative surface, rather break apart instead of absorbing further photons out of the same nanosecond laser pulse. Note that the intensity in the leading part of a nanosecond pulse is a slowly increasing function of time in comparison with the dissociation time, which can be well below 1 ps. For examples see [14] and also Section 12.3.2.

(c) For laser pulses which are short compared with the vibrational period, the corresponding spectral width is large enough to form a coherent superpositon of the vibrational states, thus forming a vibrational wave packet with a classical period $T(v+1, v) = 1/\Delta(v+1, v)$ where $\Delta(v+1, v)$ is the energy spacing of two adjacent vibrational states (in Hz). On the timescale of a few vibrational periods, the spreading of the wave packet due to the anharmonicity of real molecular potentials (see Section 12.3.1.2.4) is negligible and the dynamics of the vibrational wave packet corresponds to the classical motion of the nuclei. Therefore classical considerations can be applied, often leading to a simpler, and more direct interpretation of the data, as will be seen in Section 12.3.1.2.1.

(d) In recent years it has been shown experimentally that frequency spectroscopy can be performed using time-domain data by applying a fast Fourier transform (FFT) [15, 16]. One of the advantages of this approach arises from the differences of approximately two orders of magnitude in the timescales for vibrational motions and rotational motions. On a short timescale (a few picoseconds) only the vibrational behavior shows up in the pump-probe signal, whereas for rotational information time delays of hundreds of picoseconds have to be measured.

(e) By monitoring the changes in the femtosecond REMPI transients as a function of the excitation intensity, the dynamics in higher-lying electronic states can be separated from the dynamics in the lower states.

In addition, at higher laser intensities a wave packet in the ground state of the system can be created and the time-delayed probe laser then monitors the dynamics in the ground state as well. Both effects have been studied in the Na_2 system [17]. Recently this technique was applied to study the multiphoton dynamics of the excited states of IHgI [18].

Femtochemistry in the gas phase, introduced by Zewail and coworkers [3], is a rapidly growing field, where the one-photon pump and one-photon probe process is usually monitored by laser-induced fluorescence (LIF). The recently employed REMPI technique is increasing in importance because of the benefits described above. In order to investigate the basic mechanisms of MPI of a molecule on a femtosecond timescale we have chosen Na_2, a simple diatomic alkali metal, because of the extensive spectroscopic information available, making it easy to compare the results obtained in the time domain with the frequency-domain results. In Chapter 12.3.1.2 we focus on the Na_2 dimer and we discuss the physics of the various observations from a classical point of view. The quantum-mechanical treatment of our fs pump–probe experiments on Na_2 is given in Chapter 11.

We performed the experiments described in Sections 12.3.1 and 12.3.1.8 with identical pump and probe pulses extracted from the amplified fundamental of the CPM laser around 2 eV. This has the advantage of a precise zero delay-time determination, which is useful for example, for measuring phase shifts with respect to time-zero. Moreover, since many nanosecond laser REMPI experiments are performed with one color, the additional new information extracted from time-domain experiments are more directly related to the nanosecond REMPI work when using identical femtosecond pump and probe laser pulses.

12.3.1.2 Na_2

12.3.1.2.1 Multiphoton Ionization

Three photons with a photon energy around 2 eV are needed to ionize the Na_2 molecule. As we perform our experiments in a supersonic molecular beam, we start in $v'' = 0$, the lowest vibrational level of the $X\,^1\Sigma_g^+$ ground state [19] of the molecule. Absorption of one photon excites the $A\,^1\Sigma_u^+$ state [20], whereas absorption of a second photon excites the $2\,^1\Pi_g$ state [21]. The third photon will ionize the molecule into the ionic ground state $^2\Sigma_g^+$ [22]. Typical vibrational periods at these excitation energies are around 300 fs. The employed laser pulses in the range 70–110 fs are considerably shorter than these vibrational periods. In order to study the dynamics of this MPI, we performed a pump-probe experiment using these ultrashort laser pulses and measured the Na_2^+ yield as well as the Na^+ yield as a

function of delay time. The results obtained with light pulses of 85 fs duration and centered at 623 nm are displayed in Fig. 12.4. First we focus on the discussion of the Na_2^+ transient. This transient is symmetric with respect to time-zero, because of the identical pump and probe laser pulses. There is a pronounced oscillatory structure that shows no phase shift with respect to time-zero as indicated by the broken lines.

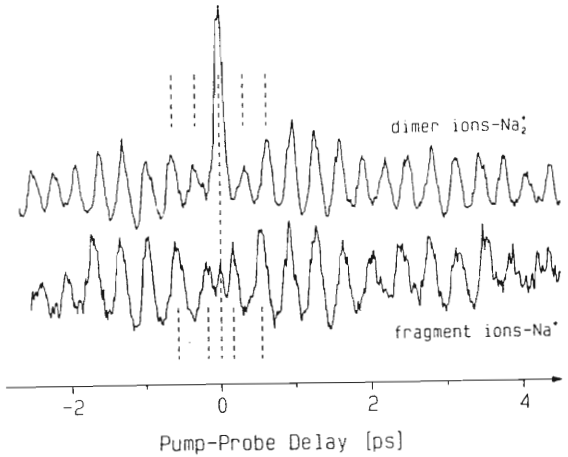

Figure 12.4 Upper trace: transient Na_2^+ signal obtained as a function of pump–probe delay time between two identical femtosecond laser pulses with 85 fs at $\lambda_{max} = 623$ nm. The envelope intensity variation and the oscillatory structure of this transient Na_2^+ MPI signal reveal two contributions out of phase by 180°. They correspond to independent wave-packet motions in bound molecular potentials with oscillation periods of 309 fs ($A\,^1\Sigma_u^+$) and 362 fs ($2\,^1\Pi_g$). Lower trace: transient Na^+ fragment signal, obtained under the same experimental conditions as the Na_2^+ transient, showing the dynamics of the 180° phase-shifted $2\,^1\Pi_g$-state wave-packet motion.

From the beat structure seen in the Na_2^+ transient, it is evident that there is at least a second oscillating contribution to the signal being out of phase by 180° as the beat envelope starts with a minimum at zero delay time.

The origin of the pronounced structure with no phase shift is easily understood by looking at the potential energy diagram of the molecule (Fig. 12.5). The MPI is divided into a one-photon pump and two-photon probe scheme. The pump photon prepares a wave packet at the inner turning point of the $A\,^1\Sigma_u^+$ state by a coherent superposition of a number of vibrational states. For the central wavelength of 623 nm we calculate, on the basis of the known spectroscopic constants of the $A\,^1\Sigma_u^+$ state, a vibrational period of 308.6 fs, in perfect agreement with the 309 fs ± 3 fs obtained directly from the Na_2^+ transient in Fig. 12.4. This wave-packet motion is transferred into the ionization continuum by the two probe photons at the *inner* turning point in each round trip, as there is no phase shift observed with

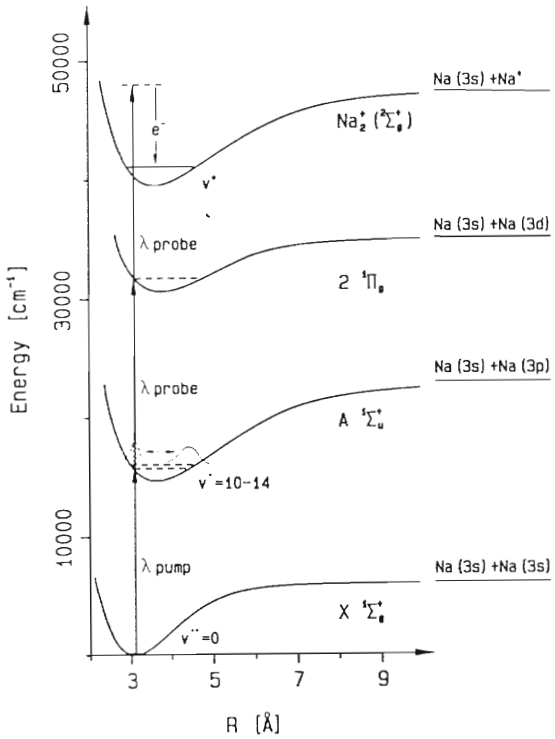

Figure 12.5 Scheme for a one-photon pump and two-photon probe direct ionization. The potential energy curves for the involved electronic states are shown. The pump pulse prepares a coherent superposition of vibrational states in the electronic $A\,^1\Sigma_u^+$ state at the inner turning point. The motion of the vibrational wave packet is probed at the inner turning point by a time-delayed femtosecond laser pulse. A two-photon probe process transfers the motion into the ionization continuum via the $2\,^1\Pi_g$ state.

respect to zero delay time in the Na_2^+ transient. The first probe photon excites the $2\,^1\Pi_g$ state, whereas the second probe photon directly ionizes this Rydberg state. This is an MPI process where all three photons are absorbed simultaneously within the temporal overlap of pump and probe pulses. There is one question remaining to be addressed: Why do all the excitation steps of this MPI process occur mainly at the inner turning point? This can be discussed by classical arguments, as wave packets are well localized in space and their time evolution is the quantum-mechanical counterpart to the classical motion of the nuclei. We applied Mulliken's concept of difference potential [23] to the interpretation of our results. The basic idea is that an electronic transition does not influence the kinetic energy of the nuclei. This leads to the condition that the intersection of the excitation energy with the difference potential of the two potential energy surfaces involved determines the

classical transition regions. This is illustrated in Fig. 12.6, where the $A\,^1\Sigma_u^+ - X\,^1\Sigma_g^+$ transition is given as an example. It is clearly seen that the excitation with a pump photon creates a wave packet at the inner turning point of the $A\,^1\Sigma_u^+$ state. By treating the two-photon probe transition in the same manner [24], it is understood why the wave-packet motion is seen in phase with the preparation at the inner turning point for zero delay time. It is the resonance-enhancing $2\,^1\Pi_g$ state that restricts the probe transition to a "window"-region near the inner turning point. A full quantum-mechanical treatment and the comparison with the experiment is given in [25].

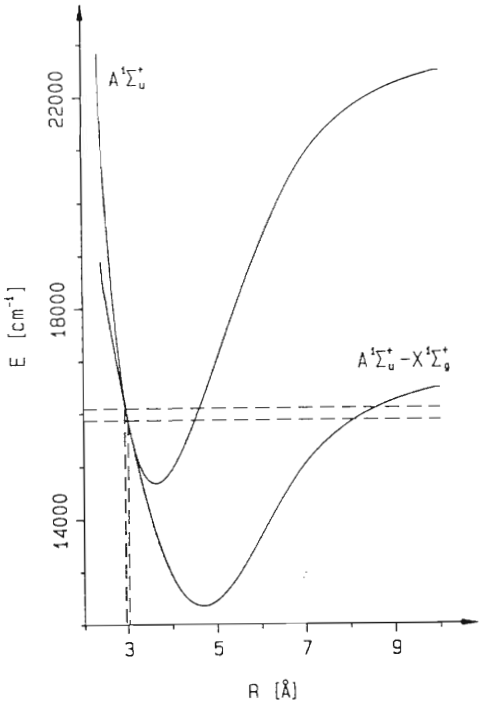

Figure 12.6 The difference potential $A\,^1\Sigma_u^+ - X\,^1\Sigma_g^+$ is shown together with the $A\,^1\Sigma_u^+$ state of Na_2. The broken horizontal lines indicate the bandwidth of the pump laser at the excitation wavelength. The intersection with the difference potential determines the classical transition region (vertical broken lines). For our pump-pulse photon energy, the coherent excitation of v' levels occurs within a narrow range of internuclear distances at the inner turning point of the $A\,^1\Sigma_u^+$-state potential.

The period of the second oscillating contribution of the Na_2^+ transient was determined by an FFT to 362 fs. This is the classical round-trip time of a wave packet in the $2\,^1\Pi_g$ state of the molecule at the excitation energy of two pump photons. As we know from the data, this wave packet is phase-shifted by 180° with respect to zero delay time. Thus this wave packet is coupled into the ionization continuum at the outer turning point of the $2\,^1\Pi_g$ state. The analysis of this transition with the difference potential concept [24] and also quantum-mechanically [26] showed the surprising result that direct ionization with one probe photon of the $2\,^1\Pi_g$ state gives

a time-independent Na_2^+ signal. On the basis of these findings, the 180° phase shift and the time-resolved Na^+ photofragmentation, we concluded that in this ionization process the excitation of a neutral, doubly excited bound state of the Na_2 molecule is involved with its subsequent decay channels (see Fig. 12.7):

(a) electronic autoionization, leading to the observed phase-shifted $2\,^1\Pi_g$ wave-packet motion in the Na_2^+ transient, and
(b) electronic autoionization-induced fragmentation via the repulsive $^2\Sigma_u^+$ state [27], leading to slow ionic fragments which show the $2\,^1\Pi_g$ oscillation period and the 180° phase shift directly in the Na^+ transient.

The proof of this interpretation is given by the lower trace in Fig. 12.4, where the Na^+ transient indeed shows the anticipated behavior. Note that the broken curve representing the doubly excited neutral state in Fig. 12.7 is an estimated potential curve.

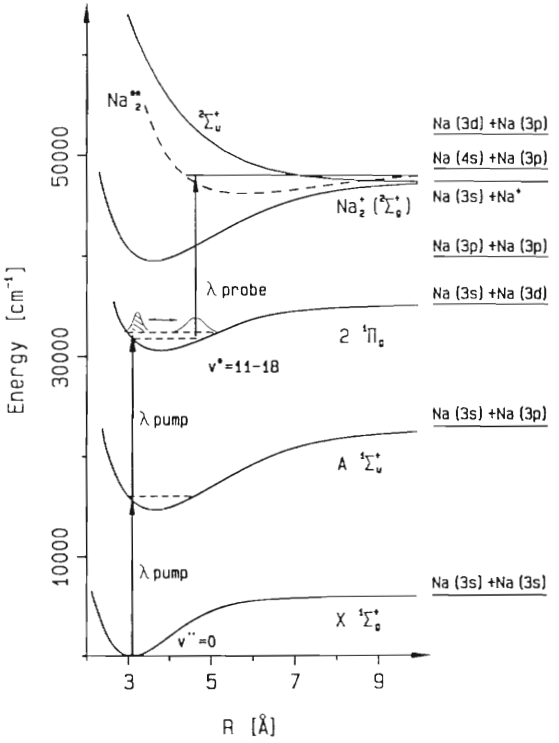

Figure 12.7 Ionization scheme for a two-photon pump transition to the electronic $2\,^1\Pi_g$ state and an indirect one-photon ionization which proceeds via excitation of a bound, doubly excited state of Na_2 and subsequent electronic autoionization. The broken line is an estimate for the potential curve of Na_2^{**}. The probe process occurs only at the outer turning point due to the 180° phase shift of the $2\,^1\Pi_g$ wave-packet motion seen in Fig. 12.4.

Recent calculations of doubly excited states by Meyer [28] give a $^1\Pi_u$ state in that energy region which can be excited from the outer turning point of the $2\,^1\Pi_g$state [29]. Note that in this MPI process the photons are absorbed sequentially: at the earliest, after half a vibrational period of the $2\,^1\Pi_g$ state, the third photon is absorbed.

In the Section 12.3.1.2.2 we discuss an important question connected with the fact that the ratio of observed sodium dimer ions and atomic ions is modulated strongly as a function of pump-probe delay time.

12.3.1.2.2 Control of Na_2^+ Versus Na^+ Yield

Controlling a chemical reaction so that a given product is produced at the expense of another (energetically allowed) product is one of the basic issues in physical chemistry. Many publications are devoted to this topic. Some references can be found in a recent review by Warren *et al.* [30]; see also Chapters 2 and 23–26. In larger molecules the locally deposited energy redistributes very rapidly throughout the molecule, so specially designed pulse shapes and phase shifted pulses are currently being discussed to be used in order to achieve bond selectivity in these systems. For smaller molecular systems, however, the basic ideas of the Tannor–Kosloff–Rice scheme [31] are applicable. They have proposed that controlling the duration of propagation of a wave packet on an excited electronic potential energy surface, by simply controlling the time delay between pump and probe pulses, can be used to generate different chemical products on the ground-state potential energy surface. This idea of controlling the duration of propagation of a wave packet on an excited electronic surface was realized in an experiment by Zewail and coworkers [32]; see also Chapter 2. They used two sequential coherent laser pulses to control the reaction of I_2 molecules with Xe atoms to form XeI. It was shown that the yield of product XeI is modulated as the delay between the pulses is varied, reflecting its dependence on the nuclear motions of the reactants. However, for the first time (to our knowledge) an example of how the propagation of wave packets can be used to produce one product at the expense of another, energetically allowed, product is given by our experiments:

To clarify this topic, let us assume that we focus a nanosecond laser on our molecular beam having a photon energy of about 2 eV. After absorption of three photons, we will detect Na_2^+ and Na^+ in our TOF spectrometers according to the two ionization processes described before. There are no simple means to produce Na_2^+ at the expense of Na^+ with this nanosecond laser at a fixed intensity and wavelength. Using the time-resolved approach, we know that at the inner turning point of the $A\,^1\Sigma_u^+$ and $2\,^1\Pi_g$ states in Na_2 the molecule is directly ionized by the probe laser (see Fig. 12.5), whereas only at the outer turning point of the $2\,^1\Pi_g$ state are fragment ions Na^+ produced by exciting the doubly excited state with its subsequent decay channels (Fig. 12.7). Thus, by controlling the duration of propagation of the wave packets on the $A\,^1\Sigma_u^+$ and $2\,^1\Pi_g$ states in Na_2, we are able to produce Na_2^+ at the expense of Na^+ by adjusting the pump-probe delay time. This is illustrated in Fig. 12.8, where the ratio of the Na_2^+ signal to the Na^+ signal from

Fig. 12.4 is displayed. A modulation of this ratio by a factor of at least 2 is seen as a function of pump-probe delay. It should be noted that, even for delay time $\Delta t = 0$, ionic fragments are formed through different processes – either by further absorption of photons due to the higher laser intensity at $\Delta t = 0$, or by the processes described in [1].

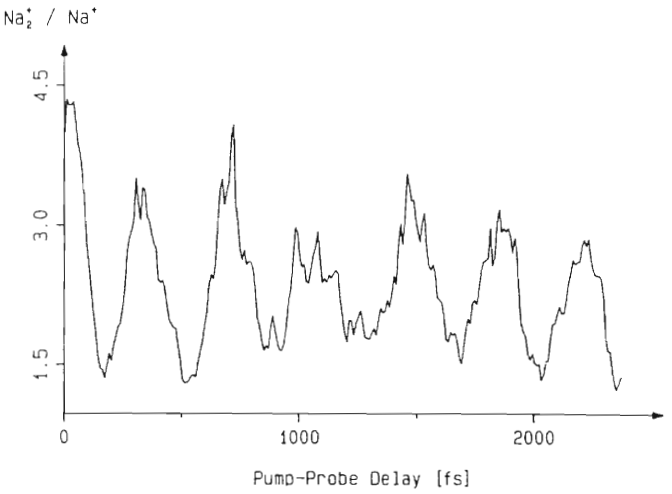

Figure 12.8. Controlling the production of Na_2^+ versus Na^+ in a Tannor–Kosloff–Rice-like scheme by adjusting the pump-probe delay time and therefore controlling the internuclear distance of the molecule.

12.3.1.2.3 Interaction with High Laser Fields: Ground-State Wave Packet

The experiments described above were performed with attenuated laser intensity, because we were interested in the basic MPI processes. In this section we describe the dependence of the total Na_2^+ ion signal on the intensity of the femtosecond pulses. A detailed discussion can be found in [17]. The experimental results shown in Fig. 12.9a were obtained for three different intensities ($I_0 = 10^{12}$ W cm^{-2}, 0.3 I_0 and 0.1 I_0). The curves exhibit periodic oscillations with different periods for different laser intensities. The periodic contributions to these transients were analyzed by taking their Fourier transform, displayed in Fig. 12.9b. For higher laser intensities, the relative contributions from the $A\,^1\Sigma_u^+$ and the $2\,^1\Pi_g$ states change dramatically. In addition, for the strongest fields used in these experiments a frequency distribution around 157.5 cm^{-1} is seen in the Fourier transform. The vibrational spacings in the $X\,^1\Sigma_g^+$ ground state of Na_2 are 157.7 cm^{-1}, 156.2 cm^{-1} and 154.7 cm^{-1} ($v'' = 0$–3) [19]. As these large vibrational spacings exist for only the ground state in the Na_2 system, we conclude that a vibrational wave packet in the

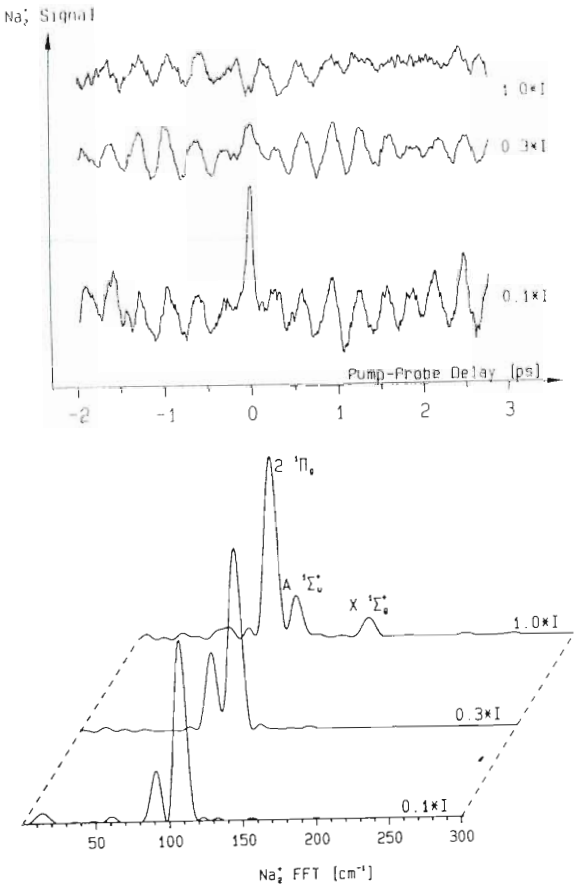

Figure 12.9 (a) Transient Na_2^+ spectra as a function of delay time between pump and probe pulses. Different intensities were used as indicated. (b) Fourier transforms of the transient spectra. Note the dramatic change of the Fourier amplitudes as a function of intensity. At $1.0 \times I$ a contribution of the $X\,^1\Sigma_g^+$ ground-state wave packet to the transient ionization spectrum is observed in the Fourier spectrum.

electronic ground state $X\,^1\Sigma_g^+$ is created through stimulated emission during the time when the ultrashort pump pulse interacts with the molecule. Such a process was anticipated theoretically by Hartke *et al.* in the CsI system [33]. This ground-state wave-packet dynamics is monitored by absorption of three photons from the time-delayed probe laser in a direct photoionization process.

Time-dependent quantum calculations were performed to explain this behavior (see [17] and Chapter 11). They show that, for different laser field strengths, the electronic states involved in the MPI and coupled coherently by the laser interaction are populated differently in a Rabi-type process. For lower intensities the $A\,^1\Sigma_u^+$ state is preferentially populated by the pump pulse and the $A\,^1\Sigma_u^+$ wave-packet motion dominates the ion signal. For the highest intensity used in these experiments, the contribution of the $2\,^1\Pi_g$ state motion dominates. This is because, after the pump pulse is over, the $2\,^1\Pi_g$ state is more populated than the $A\,^1\Sigma_u^+$ state. The population in the $A\,^1\Sigma_u^+$ state is initially increasing with the rising part of the pump pulse, but then the Rabi-type process starts to decrease the population again. This behavior is sketched in Fig. 11.7 for three different laser intensities. Thus, by changing the intensity of the laser, one may selectively control the relative contribution of the direct one-electron photoionization versus the two-electron excitation and electronic autoionization process to the total signal. This intensity-dependent effect will be used in future experiments to optimize the control scheme of Section 12.3.1.2.2.

12.3.1.2.4 Long-Time Behavior of a Vibrational Wave Packet

We have seen that the initial wave-packet motion in the bound state of a diatomic nicely represents the classical motion of the two nuclei against each other (Section 12.3.1.2.2), where the oscillation time is roughly given by the inverse of the vibrational spacing excited by the centre wavelength (for a more exact determination the spectral distribution of the laser pulse, the transition dipole moment and Franck–Condon considerations have to be taken into account). This classical motion, however, is only seen for a couple of vibrational periods, as the anharmonicity of real molecular potentials causes a spreading of this oscillatory motion for longer evolution times of the wave packet. This spreading happens in a well-defined way and the wave packet restores completely after a certain time, as will be shown. We describe the long-time behavior of a vibrational wave packet in this section by classical means and we take the wave-packet motion in the $A\,^1\Sigma_u^+$ state as an example. At low laser intensities, the Na_2^+ transient is dominated by the oscillating contribution of the $A\,^1\Sigma_u^+$ state wave-packet motion due to the direct photoionization process described above. Using the femtosecond pump–probe technique, we are therefore able to study the long-time behavior of a vibrational wave packet.

The spreading and recurrence are basically given by the anharmonicity of a real diatomic molecular potential: there the energy splitting $\Delta(v+1, v)$ varies as a function of v. Thus the classical oscillation periods $T(v+1, v) = 1/\Delta(v+1, v)$ will change with the vibrational quantum number v. For three vibrational levels and the assumption that $T(v+1, v) > T(v, v-1)$, the phase of the wavefunction will resemble that for time $t = 0$ if $kT(v+1, v) = (k+1)\,T(v, v-1)$, where k counts the number of periods which have passed. This defines the recurrence time (for a more general discussion, see [34]):

Taking the known spectroscopic constants of the $A\,^1\Sigma_u^+$ state [20] into account, we can

$$T_{\text{rec}} = \frac{T(v+1, v)\,T(v, v-1)}{T(v+1, v) - T(v, v-1)} \tag{1}$$

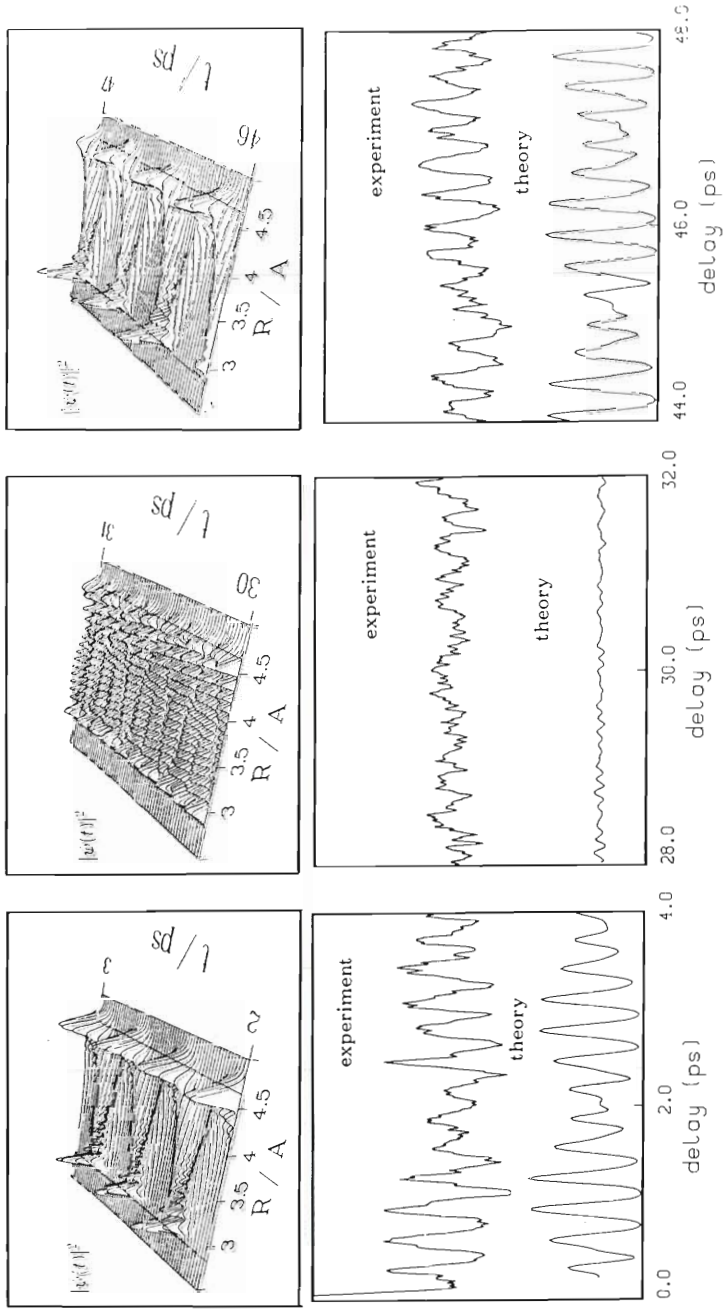

Figure 12.10 'Snapshots' of long-time behavior of the $A\,^1\Sigma_u^+$-state wave packet at three different times. The upper diagrams show in each case the dynamics of this vibrational wave packet. The straight lines parallel to the time axis indicate the classical turning points corresponding to the average energy of the packet. In each lower plot, the measured pump–probe ionization signal is shown as a function of delay time between the laser pulses and compared with the calculated total ionic population. (a) Initial dynamics of the wave packet after 2 ps. (b) Spreading of the wave packet after 30 ps. (c) Complete recurrence of the wave packet at 47 ps delay time.

calculate a recurrence time of 47 ps for laser pulses of 618 nm central wavelength, and a temporal width of 65 fs. In Fig. 12.10, 'snapshots' of the measured and calculated wave-packet dynamics in the $A\,^1\Sigma_u^+$ for three different times (2 ps, 30 ps, are shown, At early times around 2 ps the vibrational wave packet nicely illustrates the classical motion of the two nuclei. After 30 ps the wave packet is completely dispersed and fills the whole classically allowed region. At any instant of time, one finds a probability density at the inner potential region where the transition to the ion takes place. Consequently the ion signal has lost its periodic intensity variation. After 47 ps, however, the wave packet is localized as it is for short times and again it moves periodically back and forth in the bound state potential. A more detailed description of this experiment and the time-dependent quantum calculations has been provided [35].

12.3.1.2.5 Frequency Spectroscopy in the Time Domain: The Double-Minimum State $2\,^1\Sigma_u^+$

At first glance, the terms 'frequency spectroscopy' and 'time domain' seem to be contradictory because of the broad spectral distribution contained in an ultrashort laser pulse. However, the spectroscopic information can be derived from data taken in the time domain by a Fourier transformation. This has been shown for diatomics and diatomic-like molecules by Zewail's group for the systems I_2 [15] and ICN [16]; see also Chapter 2. Although the time-resolved approach cannot compete with the elaborate techniques of high-resolution spectroscopy for bound systems, for predissociating or dissociative systems this approach might sometimes be the only choice in order to determine spectroscopic data, especially in the transition-state region. Another advantage of the time-resolved method is the ease of distinction between vibrational and rotational spectroscopic information, because their energy spacings (e.g., oscillation periods) are different in general by two orders of magnitude. For bound systems the achievable resolution is limited only by the scan length. Using a square window in the Fourier transformation, the theoretical resolution limit for the full width at half-maximum (FWHM) is 0.1 cm^{-1} for a scan length of 300 ps. Note that peak positions (frequencies) in such an FFT spectrum can be determined with higher accuracy.

In this section we take the $2\,^1\Sigma_u^+$ state [36, 37] of Na_2 as an example to illustrate this fact. The double-minimum structure of this state (see Fig. 12.11) is formed by the avoided crossing of two adiabatic potential curves. The first of these is a Rydberg state and the second has substantial ionic character at large internuclear distances [36]. The principle idea of this experiment is sketched in Fig. 12.11. A pump pulse at 340 nm prepares the wave packet at the inner turning point of the $2\,^1\Sigma_u^+$ state above the barrier. The probe laser is tuned to 540 nm in order to transfer the wave packet onto the repulsive $^2\Sigma_u^+$ ionic curve only at the outer turning point of the double-minimum state. The time-resolved detection of the slow atomic Na^+ fragments will therefore reflect the vibrational wave-packet motion in the $2\,^1\Sigma_u^+$ double-minimum state of the molecule. A detailed description of the very interesting MPI processes has been given elsewhere [38].

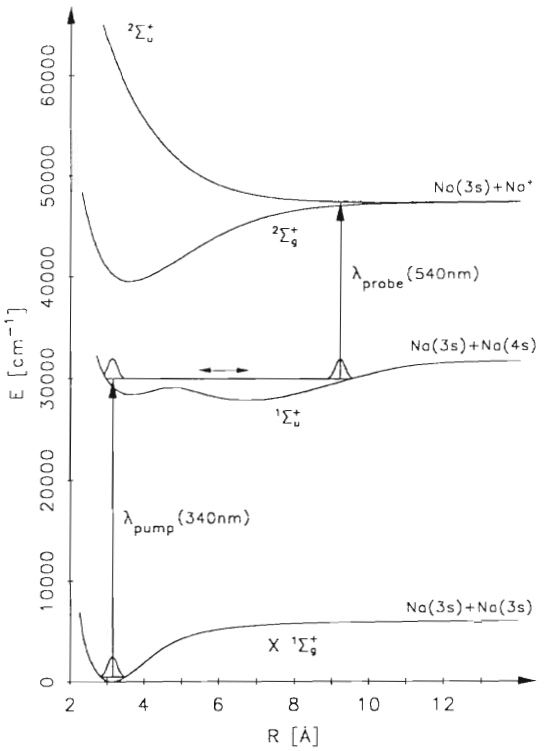

Figure 12.11 Potential energy diagram illustrating the basic idea of the double-minimum experiment. The pump pulse creates a wave packet the inner turning point of the $2\,^1\Sigma_u^+$ potential. The probe laser is tuned so that the wave packet is transferred only at the outer turning point into the $^2\Sigma_u^+$ repulsive ionic continuum.

The connection of resolution in the frequency domain and scan length in the time domain is demonstrated in Figs 12.12 and 12.13. Figure 12.12a shows the dynamics of the wave packet monitored on the slow atomic Na^+ fragments for a scan length up to 12 ps. The oscillatory behavior of the wave packet, as well as the onset of the spreading due to the anharmonicity of this potential, is clearly seen. The FFT of this transient (not shown) gives a frequency distribution centered around 33.4 cm^{-1} (1 ps), where the individual vibrational energy spacings contained in the wave packet are not resolved. In 12.12b the first 40 ps of an Na^+ transient 170 ps long is displayed. The spreading of the wave packet is obvious. An FFT of this transient shows only frequencies in the range 33–35 cm^{-1}, as shown in the upper part of Fig. 12.13a. By zooming into this frequency range (Fig. 12.13b), it is shown that this frequency distribution is composed of a number of individual frequencies. These frequencies are indeed the vibrational energy spacings of which the wave packet is

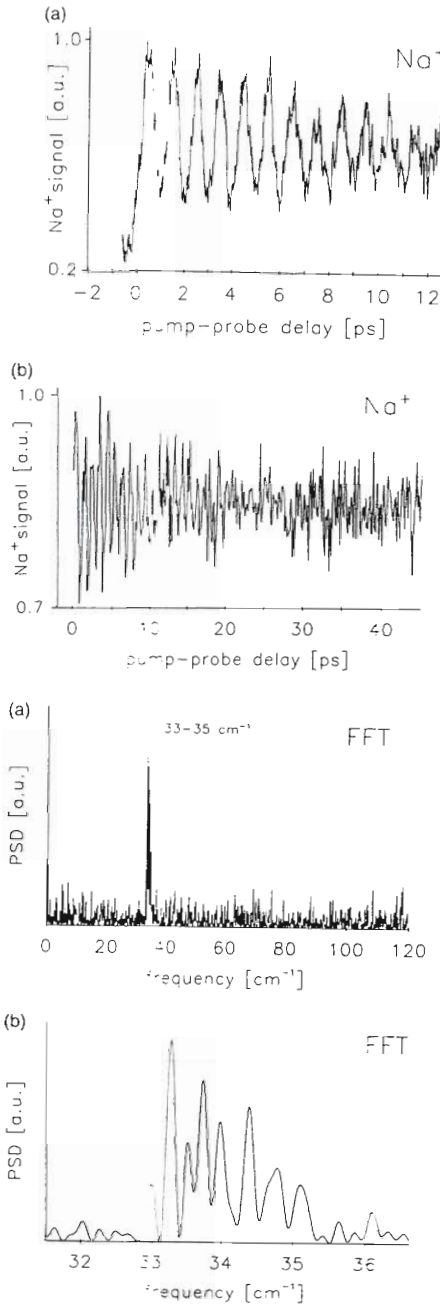

Figure 12.12 (a) Na^+ transient obtained in the excitation scheme of Fig. 12.11, showing the oscillatory motion of the wave packet in the $2\,^1\Sigma_u^+$ state of Na_2 for the first 12 ps. (b) First 40 ps of a 170 ps Na^+ transient obtained in the pump–probe scheme of Fig. 12.11. The spreading of the wave packet is clearly seen.

Figure 12.13 (a) Fourier transformation of the transient shown in Fig. 12.12b. Only frequencies in the range 33–35 cm^{-1} contribute to the formation of the wave packet. (b) Enlargement of the Fourier transformation in (a). The frequency distribution is composed of individual frequencies corresponding to the energy spacings of the vibrational levels forming the wave packet.

composed, as may be seen by comparing these time-domain results with high-resolution results obtained by Cooper *et al.* [36] (see Table 12.1). The nanosecond laser REMPI results of Hertel and coworkers [39] and Delacretaz and Wöste [40] are also shown for comparison.

Table 12.1 Vibrational energy spacings $\Delta G(v)$ obtained by Fourier transformation of femtosecond time-domain measurements shown in Fig. 12.12.

v'	REMPI[(b)] cm^{-1}	REMPI[(c)] cm^{-1}	FTS[(d)] cm^{-1}	Femtosecond experiment cm^{-1}
59-58	–	–	35.19	
58-57	–	–	35.06	35.1
57-56	35.1	35.5	34.91	
56-55	34.1	34.0	34.75	34.78
55-54	34.5	35.4	34.58	34.65 (s)
54-53	34.8	34.4	34.39	34.39
53-52	33.8	33.5	34.20	34.16 (s)
52-51	34.5	34.7	33.99	33.98
51-50	35.9	35.4	33.76	33.73
50-49	31.5	33.4	33.53	33.51
49-48	33.3	31.6	33.28	33.27
48-47	33.4	33.7	33.00	33.00
47-46	32.5	33.0	32.71	–
46-45	32.5	33.1	32.40	–

[(a)] The symbol s denotes values obtained from shoulders in Fig. 12.13. The assignment to v' levels in the $2\ ^1\Sigma_u^+$ state is based upon high-resolution Fourier transform spectroscopy (FTS) data. Results of nanosecond laser REMPI experiments are also given.
[(b)] From [40].
[(c)] From [39].
[(d)] From [36].

12.3.1.3 Related Experiments on Other Alkali-Metal Diatomics

There are, to our knowledge two other research groups who have recently started to investigate the wave-packet motion in molecular multiphoton ionization of alkali-metal diatomics. In the Cs_2 system, the dynamics of vibrational wave packets in the weakly predissociated $C\ ^1\Pi_u$ state has been measured by Rodriguez and Eden [41] in a two-color femtosecond pump-probe experiment, recording the time and energy-integrated photoelectron signal with a proportional counter in a cell. They explained the decreasing v' excitation with increasing photon energy by an interplay of the thermal distribution in the ground state with Franck-Condon arguments. The K_2 system is being investigated by Wöste and coworkers [42]. The transient K_2^+ signal as a function of pump-probe delay is displayed in Fig. 12.14. This transient, obtained at a central wavelength of 840 nm, is similar to our observed transient Na_2^+ signal (Fig. 12.4a). Using the difference potential concept and quantum-mechanical

calculations, the observed dynamical features of that experiment are still under evaluation. However, since Na_2 and K_2 are very similar and their transients are very much alike, it is expected that the basic physical processes observed with Na_2 also play a role in K_2 multiphoton ionization. For instance, the observed 380 fs oscillation period in Fig. 12.14 is interpreted by Wöste and his group as a ground-state wave-packet motion [43].

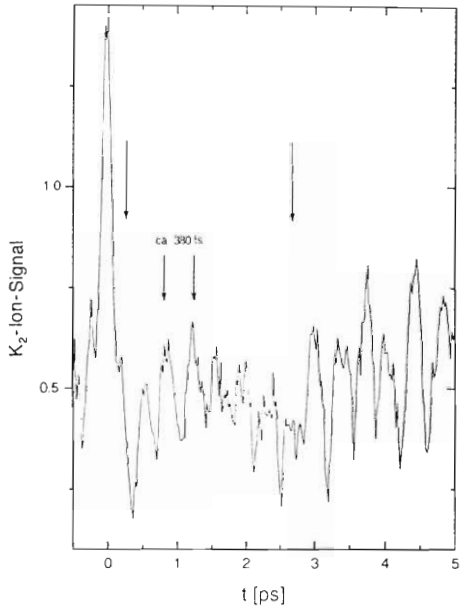

Figure 12.14 K_2^+ ion signal at a central wavelength of 840 nm [43]. An oscillation period of 380 fs is observed. This figure is provided by Wöste's group in Berlin.

12.3.1.4 Three-Dimensional Wave-Packet Motion on the B State of Na_3

Until now we have investigated simple diatomics and we have seen that the wave-packet dynamics represents the classical motion of the two nuclei. Furthermore, we have shown in Section 12.3.1.3 that we can perform frequency spectroscopy in the time domain. The question that arises now is whether we can extend this concept to larger molecules. We have chosen the sodium trimer as an example. This trimer is a nonlinear molecule and therefore has three normal modes. In the wavelength range from 600 to 625 nm, excitation of the B state of this molecule occurs [2]. Delacretaz *et al.* [44] have assigned the B-state spectrum in terms of a Jahn-Teller model, whereas more recently Meiswinkel and Köppel [45] explained the spectrum by a pseudo Jahn-Teller model. The normal modes of this state are only known theoretically [46, 47]. The experiment described below is discussed in detail in [48].

We performed a pump-probe experiment with 60 fs laser pulses centered at 623 nm and detected the Na_3^+ ions as a function of delay time. The resulting transient ionization spectrum of Na_3 is displayed in Fig. 12.15a. This time-domain spectrum is more complex than that observed for the dimer Na_2 because more dynamical features are involved. But still there are distinct recognizable time patterns, such as the 320 fs separation of the major peaks, which corresponds to an energy of 105 cm^{-1}, and the dip around zero time delay caused by fragmentation by the intense laser fields at $\Delta t = 0$ formed of the Na_3^+. It is in agreement with high-resolution two-photon ionization (via the B state) spectra [44, 49] that we do not observe a decay of the B state for longer delay times up to 10 ps. As shown by

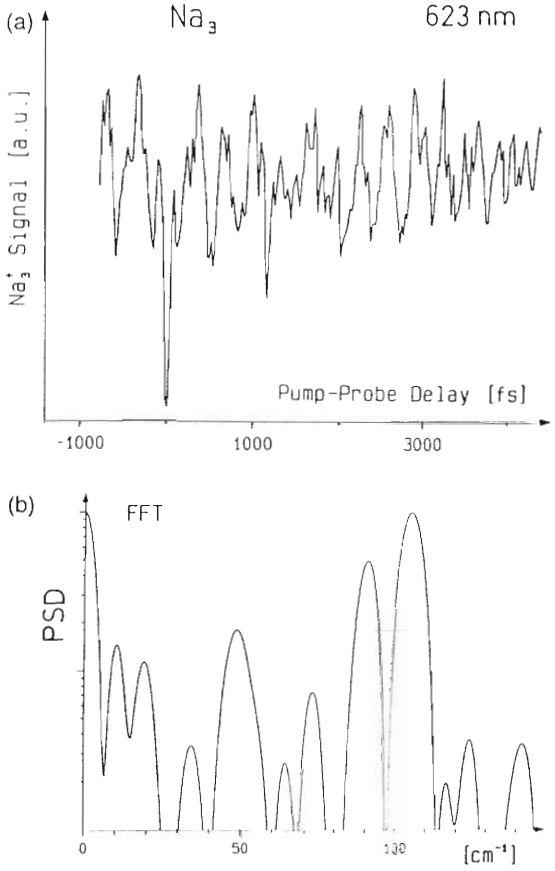

Figure 12.15 (a) Pump-probe ionization spectrum of Na_3 (X and B states) using 60 fs light pulses at 623 nm. (b) Fast Fourier transform spectrum of the Na_3 transient ionization spectrum shown in (a).

the FFT spectrum, displayed in Fig. 12.15b, the dynamics of the two-photon ionization process is determined by three-dimensional wave-packet motions in the Na_3 B state and in the X state as well. At the applied laser intensity, both states are involved. The pump laser generates a wave packet in the intermediate B state and simultaneously a wave packet in the X electronic ground state through stimulated emission pumping during the pump pulse (as was explained in Section 12.3.1.2.3 for the case of Na_2).

The contributions in the FFT spectrum (Fig. 12.15) near 140 cm^{-1}, 90 cm^{-1} and 50 cm^{-1} are attributed to the symmetric stretch, to the asymmetric stretch, and to the bending mode in the Na_3 electronic ground state. This assignment is based upon the analysis of Broyer *et al.* [50]. The wave-packet dynamics in the excited B state seems to be dominated by the symmetric stretch mode with frequencies close to 105 cm^{-1}. According to calculations by Meyer and coworkers [46] and Cocchini *et al.* [47], the eigenfrequencies of the symmetric stretch modes of the $4\,^2A_1$ and the $3\,^2B_2$ states are in the range of 94–111 cm^{-1}. The contribution around 72 cm^{-1} is tentatively assigned to the bending and asymmetric stretch modes of the $3\,^2B_2$ state.

The other observed frequencies, 8.5–12 cm^{-1}, 17.5–20 cm^{-1} and 30.5–35 cm^{-1}, are assigned according to the notation of Delacretaz *et al.* [44] to a free pseudorotational wave-packet motion in the potential surface of the B state. The energy differences of successive pseudorotational j states have been experimentally determined and assigned by Delacretaz *et al.* [44] on the basis of a pure Jahn–Teller distortion of the B state to half-integer j values; for $v = 0$, these values are set out in Table 12.2. It is however very interesting to note, that in our experiment the corresponding radial component (128 cm^{-1}) of the pseudorotational motion plays only a minor role. In contrast to this, high-resolution spectroscopy of the B–X system exhibits a strong contribution of the radial pseudorotational component. The reason for this difference is not yet fully understood; one possibility is that the employed spectral width of the pump pulse centered around 623 nm barely couples the radial vibronic levels $v = 0$ and $v = 1$. Theoretical studies by Meiswinkel and Köppel [45] showed that the observed high-resolution spectra can also be explained by taking into account a

Table 12.2 Energy differences of successive pseudorotational j states of Na_3 [44]

Δ_j	Energy difference /cm^{-1} $v = 0$	$v = 1$	from fs data
$\frac{1}{2}, -\frac{3}{2}$	2.5	5	
$-\frac{3}{2}, \frac{3}{2}$	12	13.5	8.5–12
$\frac{3}{2}, \frac{5}{2}$	18	20	17.5–20
$\frac{7}{2}, \frac{9}{2}$	34	30	30.5–35

pseudo Jahn–Teller model with integer j values. In that model the vibronic coupling of the accidentally degenerate (D_{3h}) states 3 $^2E'$ (B) and 2 $^2A_1'$ is responsible for the observed vibronic structure. So far, it is not yet clear which of the two models is more appropriate to explain the observed pseudorotational wave-packet motion, since the ultrashort dynamics depends on the pseudorotational energy *differences*. For related experiments and interpretations, see also [49, 51].

In an additional real-time experiment (see also [48]) we measured the two-photon ionization-induced zero-kinetic-energy (ZEKE) photoelectrons as a function of pump–probe delay time, using 60 fs light pulses at a wavelength of 618 nm. The fast Fourier transformation of the transient ZEKE electrons showed again the frequencies supporting vibrational wave-packet motion in the X and in the B state and the pseudorotational wave-packet motion in the B state. In this experiment the peak around 128 cm^{-1}, probably due to the B-state radial vibrational motion, is now clearly seen in contrast to the Na_3^+ Fourier transform spectrum. These differences are probably due to the different photon energies (618 nm versus 623 nm) and the different ionization processes (direct photoionization versus field ionization of high-lying Rydberg states in the case of the ZEKE experiment).

12.3.2 Sodium (Na_n) Cluster Dynamics

12.3.2.1 Femtosecond Probing of Na_n^+ Fragmentation

Recently we reported the first femtosecond time-resolved experiments in cluster physics [52], where the photofragmentation dynamics of small sodium cluster ions Na_n^+ has been studied with pump–probe techniques. The stability and fragmentation dynamics of metal cluster ions formed through laser photoionization comprise a major issue in cluster physics. In particular, for sodium and potassium cluster ions Brechignac *et al.* [53] have reported that the predominant fragmentation channels, the evaporation of neutral monomers and/or dimers, respectively, are associated with microsecond fragmentation times. They also found evidence for sequential evaporation of monomers and dimers due to cluster heating. To improve the understanding of the stability and fragmentation of metal clusters and the dynamics during and immediately after the photoionization event, and to determine the size of the ejected particle, experiments with femtosecond time resolution are performed. Ultrashort light pulses of 60 fs duration are used to photoionize the neutral sodium cluster in the beam and to induce the fragmentation. The time-delayed identical probe laser pulses photoionize the neutral photofragments ejected by the cluster ions. Time-of-flight (TOF) spectroscopy is used to determine the mass of the ion and the initial kinetic energy of the fragments ionized by the probe laser.

Figure 12.16 shows the observed transient Na_3 fragmentation spectrum. The buildup of the Na_3^+ probe signal strongly depends on the pump–probe delay time and shows a fast rise time of 0.4 ps. Because pump and probe are identical, the signal is symmetric around zero time delay. The Na_3^+ probe signal increases by about 50% within 2 ps. This experiment clearly proved that neutral Na_3 photofragments are formed and that the ejection timescale is extremely fast. As has been discussed in

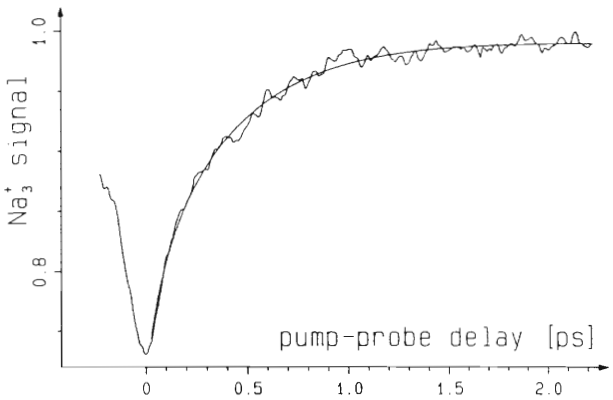

Figure 12.16 Pump–probe delay spectrum of the ejected neutral trimer fragments Na_3. The probe signal Na_3^+ buildup time constant of 0.4 ps indicates a direct photo-induced fragmentation of sodium cluster ions rather than a statistical unimolecular decay.

[52], we believe the fragmentation of Na_8^+ into Na_5^+ and Na_3 is mainly responsible for the observed neutral trimer signal. The observed rise time is too short for an efficient redistribution of the photon energy in the ionized cluster. In the discussion of the stability of metal-cluster ions against fragmentation, it is often assumed that photo-induced electronic excitation is strongly coupled and relaxed to internal modes. The excess energy from successive absorption of photons in photoionization is thought to be quickly redistributed between the vibrational modes of the cluster ion, leading to statistically dominated fragmentation. However, the observed rise time of 0.4 ps is much too fast for an efficient relaxation of energy in a cluster ion produced in a femtosecond laser interaction.

In conclusion, we find that the ejection of dimer Na_2 and trimer Na_3 photofragments occurs on ultrashort timescales of 2.5 ps and 0.4 ps, respectively. This, and the absence of cluster heating, reveal that direct photo-induced fragmentation processes, rather than the statistical unimolecular decay, are important at short times.

12.3.2.2 Femtosecond Two-Photon Ionization Spectroscopy of Na_n

Tunable femtosecond laser pulses have been applied by our group to study cluster size-dependent properties such as energy, bandwidth and lifetime(s) of intermediate resonances (Na_n^*) in beam experiments [54]. Since the complexity of the spectroscopy and dynamics of metal clusters strongly increases with the number of atoms, we have restricted our studies in the case of sodium cluster sizes to $n \leq 21$.

The cluster ion TOF spectra displayed in Fig. 12.17 are obtained under similar experimental conditions when femtosecond laser pulses with pulse energy of about 1μJ and wavelengths of 618 nm, 490 nm and 308 nm interact with the sodium cluster

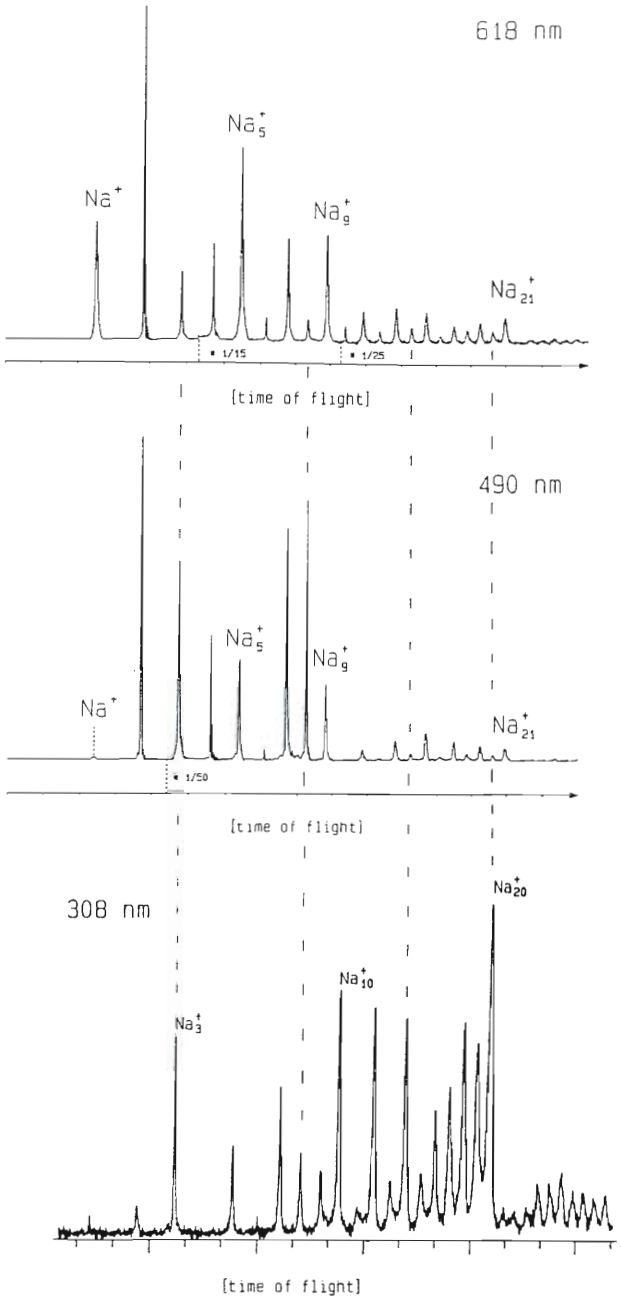

Figure 12.17 Sodium cluster ion Na_n^+ mass spectra resulting from the interaction of femtosecond laser pulses (at 1 μJ energy and of 60–100 fs pulse duration) with a sodium cluster beam. The individual cluster-ion intensities depend strongly upon the wavelength used.

beam. All three cluster size distributions look very different. Note that a cluster-ion mass spectrum resulting from an interaction of a femtosecond light pulse with a neutral cluster beam shows only parent ions and possibly ionic fragments, but is free of photoionized neutral fragments, which in nanosecond and even picosecond experiments often strongly obscure the observed spectrum. The three spectra show essentially Na_n^+ cluster sizes up to $n = 21$ in which the actual distribution is quite different in each case. Since the spectra are recorded under comparable situations, this indicates that the cluster size distributions depend strongly upon the used photon energy, i.e., on the absorption strength and energy of the intermediate electronic resonances. In the case of sodium, three 618 nm photons are needed to ionize Na_n with $n = 2$, 4, and 6, while for all other clusters with $n \geq 3$ only two photons are necessary. For 490 nm, two photons will ionize all clusters with $n \geq 3$; for 308 nm, only one photon is sufficient except for $n = 4$ and $n = 6$. It is interesting that, even with 10 times higher laser pulse intensity the relative intensities of the even- and odd-numbered clusters (for $n \geq 4$) in the ion mass spectrum do not change. This is different from findings in nanosecond experiments [55], where, for increasing laser intensities, a shift of the cluster-ion mass distribution toward lower masses has been observed which was related to cluster heating and subsequent cooling by sequential evaporation of monomers and dimers.

Note that for laser pulse durations of 60–100 fs, which are considerably shorter than the cluster vibrational periods of a few hundred femtoseconds, the clusters are nearly frozen during the photoionization event. It is therefore questionable whether cluster heating in femtosecond photoionization plays any role and whether sequential evaporative cooling occurs.

The photoabsorption spectra of neutral metal clusters are of particular interest in view of the size-dependent transition from molecule-like absorption to collective excitation of the valence electrons. For larger clusters (Na_n with $n \geq 4$) these resonances have not yet been observed in two-photon ionization spectroscopy employing nanosecond or picosecond laser pulses because of the anticipated fast decay of the intermediate Na_n^* states. However, using nanosecond laser depletion spectroscopy, Knight [56] and Kappes [57] measured these spectra for a few selected cluster sizes. We have measured the energy and bandwidth of Na_n^* ($n = 4$–21) metal cluster absorption resonances by femtosecond two-photon ionization spectroscopy in the range 1.5–3.0 eV with tunable laser pulses. The observed intermediate absorption resonances for selected neutral sodium cluster sizes ($n = 4$, 6, 8, 10 and 20) are shown in Fig. 12.18. The spectra have been obtained in the following way. Amplified femtosecond light pulses are used to generate a white-light continuum. With a variable interference filter, specific wavelengths are extracted from the continuum, amplified in a dye bow-tie amplifier and pulse-compressed. Individual two-photon ionization signals are measured every 3 or 5 nm across the dye efficiency curve. Nine different dyes had to be used to cover the energy range between 1.5 and 3.0 eV. The normalization from one dye to another was done with at least three overlapping (identical) wavelengths. For each wavelength and dye, the data were collected for a range of laser intensities (varying by a factor of 10) in order to normalize the ionization signal. Thus we knew from the slope of the ionization efficiency curve that only two photons are absorbed in the photoionization process. The displayed absorption

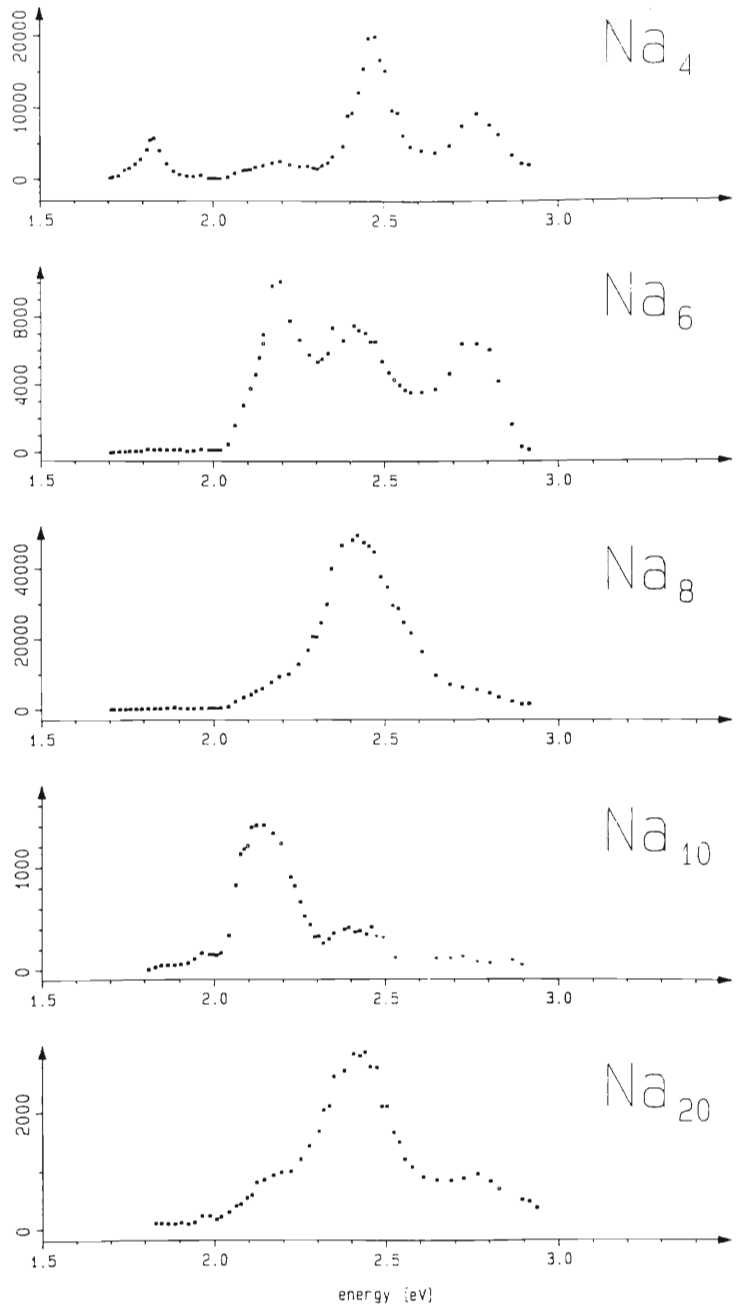

Figure 12.18 Intermediate absorption resonances for selected cluster sizes obtained by two-photon ionization spectroscopy with tunable femtosecond laser pulses. The strong resonances are in agreement with *ab initio* molecular-type calculations [62].

resonance curves in Fig. 12.18 therefore give the number of intermediate resonances and their energy for a selected neutral sodium cluster. However, the fact should not be overlooked that the data were recorded using an ultrafast light source which had an intrinsic broad spectral width in this case (about 10 nm), so we cannot exclude the possibility that there might be additional, narrower resonances underneath an absorption peak. The relative intensity of the individual resonances is much less defined because of possible variations of the relevant Franck–Condon factors, which are unknown. However, it is beyond doubt that there are several intermediate resonances, even for the closed-shell clusters Na_8 and N_{20}. This is in agreement with findings from (deconvoluted) nanosecond 'depletion spectroscopy' results of Kappes and coworkers [58]. Within the shell model [59] for the electronic structure of metal clusters the Na_8 and Na_{20} cluster sizes have a closed electronic shell and are therefore spherically symmetric. On the basis of the Jellium model, the Mie–Drude theory predicts for this spherically symmetric metallic cluster a single intense band corresponding to a classical surface-plasma oscillation. In more elaborate calculations based on random-phase approximations (RPAs) [60] or time-dependent local-density approximations (TDLDAs) [61], the photoabsorption strength (e.g., of Na_{20}) splits into two strong and several weaker peaks. However, the femtosecond two-photon ionization spectra of Na_8 and Na_{20} show several strong resonances, in agreement with *ab initio* molecular-type calculations [62], which have different bandwidths and (as discussed later) different lifetimes.

12.3.2.3 Lifetime Measurements

Measurements of the intermediate resonance lifetime(s) have been reported so far only by our group [63] and by Wöste and coworkers [64]. In our first experiments we have employed femtosecond pump–probe spectroscopy with tunable femtosecond laser pulses to measure the decay time(s) of the different absorption resonances of

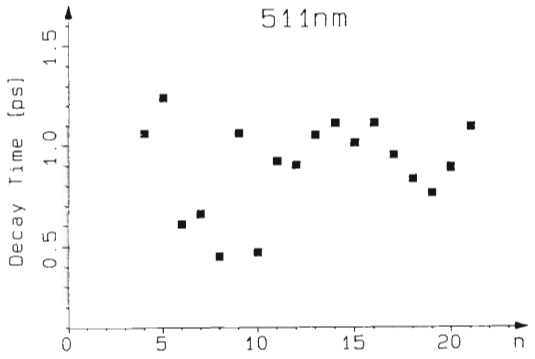

Figure 12.19 Decay times of cluster resonances at an excitation wavelength of 511 nm (where all Na_n cluster show strong absorption) as a function of cluster size, n. Selected transients are shown in Figs 12.20 and 12.21.

all Na_n cluster sizes up to $n \leq 21$. A summary of the results obtained for the strongest intermediate resonance at 511 nm (2.42 eV) is given in Fig. 12.19. The decay time of that cluster resonance varies for $n = 4$–21 between 0.4 ps and 1.2 ps with no obvious relationship to the cluster size. There is neither an even–odd variation nor an increase or decrease with cluster size apparent. And there is also no visible direct distinction between open-shell and closed-shell cluster. Theoretical estimates of lifetimes within the Mie–Drude theory give decay times of the order of 10–40 fs. Such an ultrashort decay time for a plasmon excitation has recently been observed in time-resolved measurements of the decay of a surface plasmon in a thin Ag film, where a value of 48 fs was found [65]. On the other hand, if the interaction in a metal cluster leads to a very fast distribution of the excitation energy localized in a surface plasmon into internal modes, with heating of the cluster, then the relevant statistical decay times vary strongly with cluster size. Estimated statistical unimolecular decay times would be 10 ps for Na_8 and about 10 ns for Na_{20} [56]! However, if the decay of a cluster is directly connected with a fragmentation, the relevant timescale would be of the order of a few vibrational periods, depending on the strength of interaction with a repulsive fragmentation coordinate. The observed decay times (Fig. 12.19) of 0.4–1.2 ps are of the same order of magnitude as the vibrational periods of small sodium clusters. Three examples of femtosecond pump–probe measurements in which the pump laser excites the intermediate electronic state and the time delayed probe laser monitores the time evolution of that state by ionizing the particular neutral cluster Na_5, Na_6 or Na_7 are shown in Fig. 12.20. For these measurements we employed laser pulses of 100 fs duration and a central wavelength of 511 nm. Each solid line represents a fit with a single expontential decay curve, which reproduces the measured transient very well.

Out of the large number of lifetime experiments, the results obtained for Na_{20} are particularly interesting and discussed in the following. The transient two photon ionization spectra of Na_{20}, obtained with the fs-laser tuned to the center wavelength of the 511 nm resonance is displayed in Fig. 12.21. A pump pulse of about 80 fs duration excites the Na_{20} cluster while a time-delayed identical probe pulse probes the residual population by photoionizing Na_{20}^{*}, the intermediate excited electronic state or states. As already discussed in this chapter, we have applied this technique to Na_2, Na_3 and Na_n^+ to investigate wave-packet motion and fragmentation dynamics of these systems. Figure 12.21 shows the transient Na_{20} spectrum at 511 nm, where the Na_{20}^+ signal is plotted versus the pump–probe delay time. The spectrum is symmetric with respect to zero delay time, because pump and probe pulses have the same time duration and intensity. In order to obtain the decay time constants, we have fitted the transient spectra with a sum of exponential decay functions. For the measurement at 511 nm the best fit is achieved taking into account only a single exponential with a time constant of 0.9 ps. Besides the decay, there is an additional oscillatory structure superimposed with a time period of 360 fs. An FFT of that time-domain spectrum clearly shows the corresponding frequency and some additional frequencies in the range 30–150 cm^{-1}. All these frequencies are of the order of the known vibrational eigenfrequencies of Na_3 and Na_4, as determined by ZEKE photoelectron spectroscopy [66]. Thus we believe the observed superimposed fast oscillations are

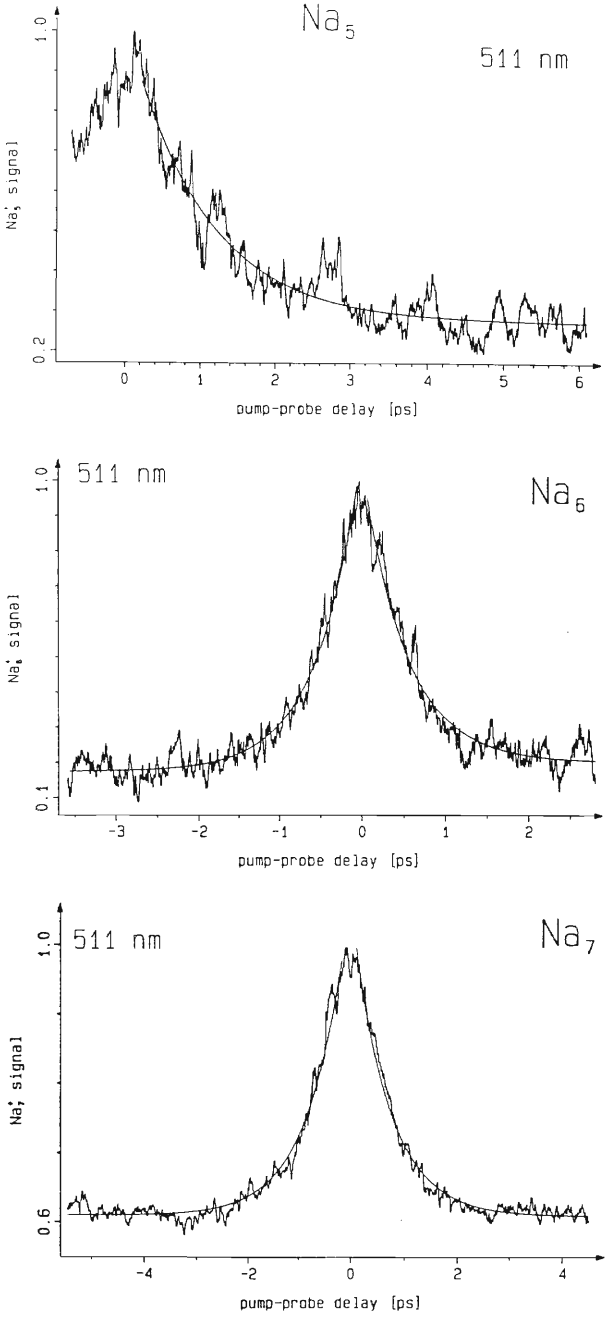

Figure 12.20 Decay of cluster resonances measured by time-delayed femtosecond two-photon ionization. Na_5, Na_6 and Na_7 are shown as examples. The transients were obtained under the same experimental conditions with laser pulses at 511 nm and of 100 fs pulse duration. The transients are fitted by a single exponential. The time constants are given in Fig. 12.19.

due to wave-packet motions in the potential surfaces of this Na_{20} metal cluster. Similar single and double exponential decay curves with superimposed oscillatory structures have been measured for other cluster sizes. A particularly good example is Na_8, where each of the observed four resonances has its own decay time(s) and exhibits a different wave-packet motion. For Na_{20} also, the decay time constants as well as the superimposed faster dynamics depend on the laser wavelength, i.e., on the specific intermediate resonance.

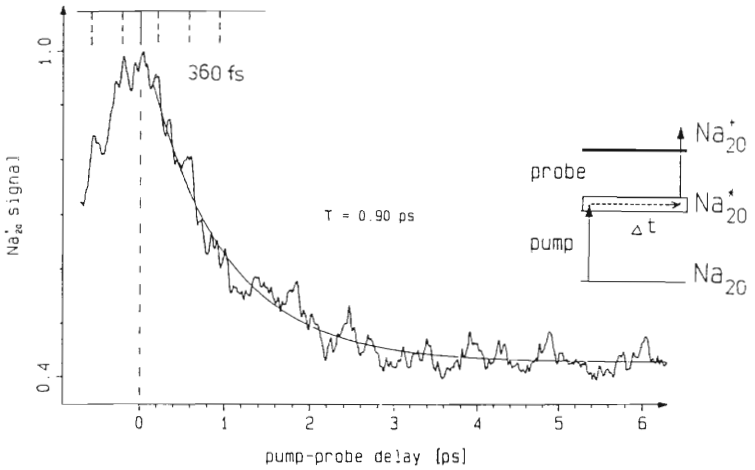

Figure 12.21 Femtosecond time resolved decay of the Na_{20}^* resonance at 511 nm. Note the oscillatory structure superimposed on the decay curve.

From these time-resolved measurements with ultrafast laser pulses it is evident that the simple picture of a surface plasmon resonance is clearly not appropriate to describe the optical excitations of small ($n \leq 21$) sodium metal clusters.

The strong wavelength dependence of the decay time constants and the superimposed fast dynamics is in agreement with the measured structure of the cluster absorption resonances. As for the cluster resonances, the pump-probe measurements are much better understood by taking into account molecular structures and excitations rather than by considering the small Na_n cluster as a metal with excitation of delocalized electrons.

On the basis of the observed cluster absorption resonances, their ultrashort lifetimes and different decay patterns, we conclude that, at least for Na_n cluster sizes with $n \leq 21$, molecular excitations and properties prevail over collective excitations and surface-plasmon-like properties.

The Wöste group in Berlin has recently reported two-color femtosecond pump-probe experiments performed with small sodium clusters in the range Na_4-Na_{10} [67]. Their technique was essentially the same as the one we have used in our experiments. A pump laser pulse excites the intermediate electronic state and a

time-delayed probe laser pulse ionizes the cluster, so that the dynamics of a single selected cluster size can be studied. In their studies they used the frequency-doubled output of a Ti:Sapphire laser at 2.94 eV to excite the cluster and the fundamental of that laser at 1.47 eV to ionize the cluster. From the pump photon energy of 2.94 eV and the information about the Na_n cluster absorption resonances given in Fig. 12.18, it is clear that they excite the cluster at the very edge of the 2.78 eV resonance. With the high repetition rate of their laser system (82 MHz) they partially compensate for the weaker absorption strength and their nJ pulse energies. Figure 12.22 shows results obtained by the Wöste group in their femtosecond pump-probe experiments. All the transients show decays on the femtosecond to picosecond timescales. From the figure, it is clear the cluster with $n = 4$ and $n = 5$, 7 and 9 exhibit a much longer decay compared with the cluster with $n = 6$, 8 and 10. This observed odd-even variation of the decay times is quite different from the result we have observed for the 2.42 eV resonance (see Fig. 12.19), where there was no obvious dependence upon cluster size, and for the 2.20 eV resonance, which decays for most of the cluster sizes on a timescale of about 350 fs. The reason for this difference in behavior of the various electronic absorption resonances is not yet fully understood.

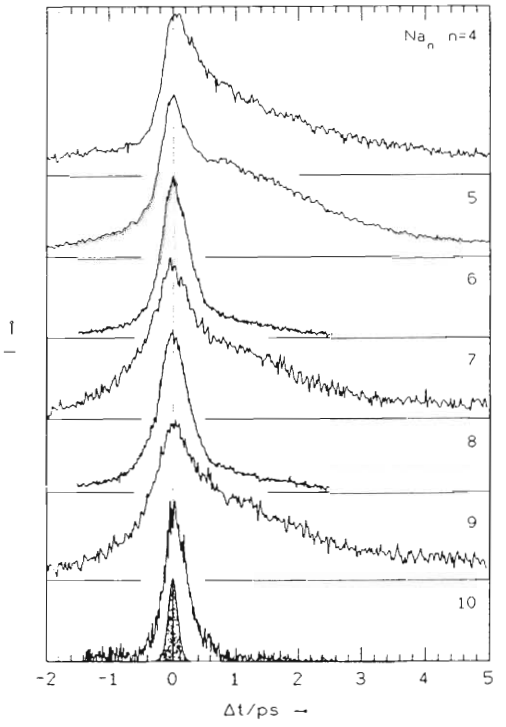

Figure 12.22 Femtosecond pump-probe measurements on Na_n cluster for $4 \leq n \leq 10$. The excitation energy is 2.94 eV. The variation of ion signal for the indicated cluster sizes is plotted against the delay time. Note the shorter decay times on $n = 6$, 8 and 10. The shaded area displayed in the lowest transient is the response function of the system [67]. This figure is provided by Wöste's group in Berlin.

12.4 Conclusion

The real-time dynamics of multiphoton ionization and fragmentation of sodium molecules and clusters, has been studied in beam experiments employing femtosecond pump-probe techniques and ion and electron spectroscopy. Time-resolved experiments with sodium dimer and trimer molecules reveal unexpected features in the dynamics of the absorption of several photons, such as the observation of a second major REMPI process in Na_2 involving excitation of two electrons and one- and three-dimensional vibrational wave-packet motions in several electronic states including the ground states. The spreading and recurrence of a vibrational wave packet in Na_2, as well as its behavior in strong laser fields, have been studied in detail.

Cluster physics bridges the gap between molecular and solid-state physics. Cluster size-dependent studies of physical properties such as absorption resonances, lifetimes and decay channels have been performed with tunable, ultrashort light pulses. On the basis of the observed number and energy of intermediate absorption resonances of individual clusters, their ultrashort lifetime(s), and different decay patterns, we conclude that the conventional view of the optical response of metal clusters, e.g., the absorption, ionization, and decay processes as well as the corresponding timescales, has to be changed. Our results clearly show that, for cluster sizes of Na_n with $n \leq 21$, the molecular structures, excitations, and properties are still important. However, it is evident that for even larger cluster the optical response must finally be dominated by collective interactions.

These real-time studies of the dynamics of ionization and fragmentation of molecules and metal clusters with femtosecond time resolution open up new and very exciting fields in molecular and cluster physics and yield results which in many cases cannot be obtained in nanosecond or picosecond laser experiments.

Acknowledgements

We gratefully acknowledge the discussions with V. Engel and C. Meier and the contributions of A. Assion, V. Gerstner, C. Rothenfusser, C. Röttgermann, V. Seyfried, S. Vogler and E. Wiedenmann to the various experiments. We also acknowledge that L. Wöste provided Figs. 12.14 and 12.22.

This work has been supported by the Deutsche Forschungsgemeinschaft through Sonderforschungsbereich 276, 'Correlated dynamics of highly excited atomic and molecular systems', in Freiburg, Germany.

Final version received: 14th March 1994

References

[1] T. Baumert, B. Bühler, R. Thalweiser, G. Gerber, *Phys. Rev. Lett.* **1990**, *64*, 733-736.
[2] M. Broyer, G. Delacretaz, P. Labastie, R. L. Whetten, J. P. Wolf, L. Wöste, *Z. Phys. D* **1986**, *3*, 131-136.
[3] L. R. Khundkar, A. H. Zewail, *Annu. Rev. Phys. Chem.* **1990**, *41*, 15-60.
[4] M. M. Kappes, R. W. Kunz, E. Schumacher, *Chem. Phys. Lett.* **1982**, *91*, 413-418.
[5] R. A. Larsen, S. K. Neoh, D. Herschbach, *Rev. Sci. Inst.* **1974**, *45*, 1511-1516.
[6] R. L. Fork, B. I. Greene, C. V. Shank, *Appl. Phys. Lett.* **1981**, *38*, 671-672.
[7] J. A. Valdmanis, R. L. Fork, J. P. Gordon, *Opt. Lett.* **1985**, *10*, 131-133.
[8] J. D. Simon, *Rev. Sci. Instr.* **1989**, *60*, 3597-3624.
[9] P. Heist, W. Rudolph, B. Wilhelmi, *Exp. Tech. Phys.* **1990**, *38*, 163-188.
[10] W. H. Knox, *IEEE J. Quant. El.* **1988**, *24*, 388-397.
[11] P. F. Curley, Ch. Spielmann, T. Brabec, F. Krausz, E. Wintner, A. J. Schmidt, *Opt. Lett.* **1993**, *18*, 54-56; M. T. Asaki, C.-P. Huang, D. Garvey, J. Zhou, H. C. Kapteyn, M. M. Murnane, *Opt. Lett.* **1993**, *18*, 977-979.
[12] R. Ogorzalek Loo, G. E. Hall, H. P. Härri, P. L. Houston, *J. Phys. Chem.* **1988**, *92*, 5; T. Baumert, B. Bühler, R. Thalweiser, G. Gerber, *Phys. Rev. Lett.* **1990**, *64*, 733-736; T. Baumert, S. Pedersen, A. H. Zewail, *J. Phys. Chem.* **1993**, *97*, 12447-12459.
[13] K. Müller-Dethlefs, M. Sander, E. W. Schlag, *Z. Naturforsch.* **1984**, *39a*, 1089-1091.
[14] D. P. Taylor, P. M. Johnson, *J. Chem. Phys.* **1993**, *98*, 1810-1816; T. Baumert, J. L. Herek, A. H. Zewail, *J. Chem. Phys.* **1993**, *99*, 4430-4440.
[15] M. Gruebele, G. Roberts, M. Dantus, R. M. Bowman, A. H. Zewail, *Chem. Phys. Lett.* **1990**, *166*, 459-469.
[16] M. H. M. Janssen, R. M. Bowman, A. H. Zewail, *Chem. Phys. Lett.* **1990**, *172*, 99-108.
[17] T. Baumert, V. Engel, C. Meier, G. Gerber, *Chem. Phys. Lett.* **1992**, *200*, 488-494.
[18] S. Pedersen, T. Baumert, A. H. Zewail, *J. Phys. Chem.* **1993**, *97*, 12460-12465.
[19] P. Kusch, M. M. Hessel, *J. Chem. Phys.* **1978**, *68*, 2591-2606.
[20] G. Gerber, R. Möller, *Chem. Phys. Lett.* **1985**, *113*, 546-553.
[21] A. J. Taylor, K. M. Jones, A. L. Schawlow, *J. Opt. Soc. Am.* **1983**, *73*, 994-998.
[22] C. Bordas, P. Labastie, J. Chevaleyre, M. Broyer, *Chem. Phys.* **1989**, *129*, 21-39.
[23] R. S. Mulliken, *J. Chem. Phys.* **1971**, *55*, 309-314.
[24] T. Baumert, B. Bühler, M. Grosser, R. Thalweiser, V. Weiss, E. Wiedenmann, G. Gerber, *J. Phys. Chem.* **1991**, *95*, 8103-8110.
[25] V. Engel, T. Baumert, Ch. Meier, G. Gerber, *Z. Phys. D*, **1993**, *28*, 37-47.
[26] V. Engel, *Chem. Phys. Lett.* **1991**, *178*, 130-133.
[27] W. Müller, W. Meyer, *J. Chem. Phys.* **1984**, *80*, 3311-3320.
[28] W. Meyer, University of Kaiserslautern, Germany, personal communication, **1993**.
[29] T. Baumert, G. Gerber, *Israel J. Chem.* **1994**, *34*, 103-114.
[30] W. S. Warren, H. Rabitz, M. Dahleh, *Science* **1993**, *259*, 1581-1589.
[31] D. J. Tannor, R. Kosloff, S. A. Rice, *J. Chem. Phys.* **1986**, *85*, 5805-5820.
[32] E. D. Potter, J. L. Herek, S. Pedersen, Q. Liu, A. H. Zewail, *Nature (London)* **1992**, *355*, 66-68.
[33] B. Hartke, R. Kosloff, S. Ruhman, *Chem. Phys. Lett.* **1989**, *158*, 238-244.
[34] I. S. Averbukh, N. F. Perelman, *Phys. Lett. A* **1989**, *139*, 449-453.
[35] T. Baumert, V. Engel, C. Röttgermann, W. T. Strunz, G. Gerber, *Chem. Phys. Lett.* **1992**, *191*, 639-644.
[36] D. L. Cooper, R. F. Barrow, J. Verges, C. Effantin, J. D'Incan, *Can. J. Phys.* **1984**, *63*, 1543-1553.

[37] J. Verges, C. Effantin, J. D'Incan, D. L. Cooper, R. F. Barrow, *Phys. Rev. Lett.* **1984**, *53*, 46–47.
[38] A. Assion, V. Seyfried, V. Weiß, E. Wiedenmann, G. Gerber, to be published.
[39] R. Haugstätter, A. Goerke, I. V. Hertel, *Z. Phys. D* **1988**, *9*, 153–166.
[40] G. Delacretaz, L. Wöste, *Chem. Phys. Lett.* **1985**, *120*, 342–348.
[41] G. Rodriguez, J. G. Eden, *Chem. Phys. Lett.* **1993**, *205*, 371–379.
[42] R. De Vivie-Riedle, K. Kobe, H. Kühling, S. Rohland, S. Rutz, E. Schreiber, L. Wöste, *Verhandlg. Dt. Phys. Gesell.* **1994**, *58*, 407.
[43] K. Kobe, Thesis Free University of Berlin, Germany, **1994**.
[44] G. Delacretaz, E. R. Grant, R. L. Whetten, L. Wöste, W. Zwanziger, *Phys. Rev. Lett.* **1986**, *56*, 2598–2601.
[45] R. Meiswinkel, H. Köppel, *Chem. Phys.* **1990**, *144*, 117–128.
[46] W. Meyer, University of Kaiserslautern, Germany, personal communication, **1993**.
[47] F. Cocchini, T. H. Upton, W. Andreoni, *J. Chem. Phys.* **1988**, *88*, 6068–6077.
[48] T. Baumert, R. Thalweiser, G. Gerber, *Chem. Phys. Lett.* **1993**, *209*, 29–34.
[49] S. Rakowsky, F. W. Herrmann, W. E. Ernst, *Z. Phys. D* **1993**, *26*, 273–275; W. E. Ernst, S. Rakowsky, *Z. Phys. D* **1993**, *26*, 270–272.
[50] M. Broyer, G. Delacretaz, G. Q. Ni, R. L. Whetten, J. P. Wolf, L. Wöste, *Phys. Rev. Lett.* **1989**, *62*, 2100–2103.
[51] J. Gaus, K. Kobe, V. Bonacic-Koutecky, H. Kuhling, J. Manz, B. Reischl, S. Rutz, E. Schreiber, L. Wöste, *J. Phys. Chem.* **1993**, *97*, 12509–12515.
[52] T. Baumert, C. Röttgermann, C. Rothenfusser, R. Thalweiser, V. Weiss, G. Gerber, *Phys. Rev. Lett.* **1992**, *69*, 1512–1515.
[53] C. Brechignac, Ph. Cahuzac, J. Ph. Roux, D. Pavolini, F. Spiegelmann *J. Chem. Phys.* **1987**, *87*, 5694–5699.
[54] T. Baumert, R. Thalweiser, V. Weiss, G. Gerber, *Z. Phys. D* **1993**, *26*, 131–134.
[55] C. Brechignac, Ph. Cahuzac, J. Leygnier, J. Weiner, *J. Chem. Phys.* **1989**, *90*, 1492–1498.
[56] K. Selby, M. Vollmer, J. Masui, V. Kresin, W. A. de Heer, W. D. Knight, *Phys. Rev. B* **1989**, *40*, 5417–5427.
[57] C. R. Wang, S. Pollak, D. Cameron, M. M. Kappes, *J. Chem. Phys.* **1990**, *93*, 3787–3801.
[58] S. Pollak, C. R. Chris Wang, M. M. Kappes, *J. Chem. Phys.* **1991**, *94*, 2496–2501.
[59] V. V. Kresin *Phys. Rep.* **1992**, *220*, 1–52.
[60] C. Yannouleas, R. A. Broglia, *Phys. Rev. A* **1991**, *44*, 5793–5802.
[61] W. Ekardt, *Phys. Rev. B* **1985**, *31*, 6360–6370; W. Ekardt, Z. Penzar, *ibid.* **1991**, *43*, 1322–1330.
[62] V. Bonacic-Koutecky, P. Fantucci, J. Koutecky, *J. Chem. Phys.* **1990**, *93*, 3802–3825; *idem, Chem. Rev.* **1991**, *91*, 1035–1108.
[63] T. Baumert, R. Thalweiser, V. Weiss, G. Gerber, *Ultrafast Phenomena VIII* (Ed.: J. L. Martins, A. Migus), Springer Series in Chemical Physics, Vol. 55, Berlin **1992**, pp. 83–86; *idem, Z. Phys. D* **1993**, *26*, 131–134; R. Thalweiser, S. Vogler, G. Gerber, *Proc. SPIE* **1993**, *1858–22*, 196–206.
[64] H. Kuhling, K. Kobe, S. Rutz, E. Schreiber, L. Wöste, *Z. Phys. D* **1993**, *26*, 33–35.
[65] M. van Exter, A. Lagendijk, *Phys. Rev. Lett.* **1988**, *60*, 49–52; D. Steinmüller-Nethel, R. A. Höpfel, E. Gornik, A. Leitner, F. R. Aussenegg, *ibid.*, **1992**, *68*, 389–392; R. A. Höpfel, D. Steinmüller-Nethel, R. Rodrigues, *Phys. Scr. T*, **1993**, *49B*, 459–463.
[66] R. Thalweiser, Thesis, University of Freiburg, Germany **1993**; R. Thalweiser, S. Vogler, G. Gerber, to be published.
[67] F. H. Kühling, Thesis, Free University of Berlin, Germany **1993**.